9556 *Biochemistry* **2009,** *48,* 9556–9568
DOI: 10.1021/bi901110n

BIOCHEMISTRY
including biophysical chemistry & molecular biology
Article

Biophysical Characterization of the Iron in Mitochondria from Atm1p-Depleted *Saccharomyces cerevisiae*[†]

Ren Miao,[‡] Hansoo Kim,[§] Uma Mahendra Kumar Koppolu,[∥] E. Ann Ellis,[§] Robert A. Scott,[∥] and Paul A. Lindahl*[,‡,⊥]

[‡]*Department of Chemistry,* [§]*Microscopy and Imaging Center, and* [⊥]*Department of Biochemistry and Biophysics, Texas A&M University, College Station, Texas 77843-3255, and* [∥]*Department of Chemistry, University of Georgia, Athens, Georgia 30602-2556*

Received June 30, 2009; Revised Manuscript Received August 28, 2009

ABSTRACT: Atm1p is an ABC transporter localized in the mitochondrial inner membrane; it functions to export an unknown species into the cytosol and is involved in cellular iron metabolism. Depletion or deletion of Atm1p causes Fe accumulation in mitochondria and a defect in cytosolic Fe/S cluster assembly but reportedly not a defect in mitochondrial Fe/S cluster assembly. In this study the nature of the accumulated Fe was examined using Mössbauer spectroscopy, EPR, electronic absorption spectroscopy, X-ray absorption spectroscopy, and electron microscopy. The Fe that accumulated in aerobically grown cells was in the form of iron(III) phosphate nanoparticles similar to that which accumulates in yeast frataxin Yfh1p-deleted or yeast ferredoxin Yah1p-depleted cells. Relative to WT mitochondria, Fe/S cluster and heme levels in Atm1p-depleted mitochondria from aerobic cells were significantly diminished. Atm1p depletion also caused a buildup of nonheme Fe(II) ions in the mitochondria and an increase in oxidative damage. Atm1p-depleted mitochondria isolated from anaerobically grown cells exhibited WT levels of Fe/S clusters and hemes, and they did not hyperaccumulate Fe. Atm1p-depleted cells lacked Leu1p activity, regardless of whether they were grown aerobically or anaerobically. These results indicate that Atm1p does not participate in mitochondrial Fe/S cluster assembly and that the species exported by Atm1p is required for cytosolic Fe/S cluster assembly. The Fe/S cluster defect and the Fe-accumulation phenotype, resulting from the depletion of Atm1p in aerobic cells (but not in anaerobic cells), may be secondary effects that are observed only when cells are exposed to oxygen during growth. Reactive oxygen species generated under these conditions might degrade iron−sulfur clusters and lower heme levels in the organelle.

Mitochondria play a major role in cellular iron homeostasis, as they are sites where iron is inserted for heme biosynthesis (*1*) and where iron−sulfur clusters (ISCs)[1] are assembled (*2*). The ferrous ions used in these processes are imported from the cytosol through the Mrs3p/4p high-affinity inner-membrane (IM) transporters. Some such centers are installed into mitochondrial apoproteins, and some heme centers are exported to cytosolic targets. The cytosolic iron−sulfur protein assembly (CIA) machinery is thought to depend on the mitochondrial ISC machinery, via an arrangement involving the IM protein Atm1p. Atm1p is an ATP binding cassette (ABC) "half-transporter" (*3*) that uses the free energy of ATP hydrolysis to transport an unknown molecular species, termed "X", from the matrix to the intermembrane space (*4*, *5*). The structure of X is unknown, but an Fe chelator (*6*), an Fe/S cluster "precursor" that contains sulfur and perhaps iron (*7*), and a peptide with multiple reduced thiol residues (*4*) have all been suggested. Guarente and Mason (*8*) have suggested that mitochondrially synthesized hemes are exported and sensed in the cytosol, but the possibility that X is a heme has been discounted (*3*). Once exported into the cytosol, X has been proposed to assist the CIA machinery in cytosolic ISC synthesis and regulate cellular Fe homeostasis.

Saccharomyces cerevisiae cells lacking Atm1p have a respiratory defect as well as diminished levels of heme prosthetic groups (*3*) and cytosolic ISC-containing proteins (*7*). There is reportedly no defect in mitochondrial ISC maturation (*7*). Depletion and deletion of Atm1p also causes Fe to accumulate in mitochondria to concentrations that are 20−30 times higher than in WT controls (presuming no difference in overall mitochondrial protein concentration) (*6*, *9*). However, the form of the accumulated Fe has not been investigated by biophysical methods.

[†]This study was supported by the Robert A. Welch Foundation (A1170, P.A.L.) and the National Institutes of Health (GM084266 to P.A.L.; GM042025 to R.A.S.). Portions of this research were carried out at the Stanford Synchrotron Radiation Lightsource, a national user facility operated by Stanford University on behalf of the U.S. Department of Energy, Office of Basic Energy Sciences. The SSRL Structural Molecular Biology Program is supported by the Department of Energy, Office of Biological and Environmental Research, and by the National Institutes of Health, National Center for Research Resources, Biomedical Technology Program.

*To whom correspondence should be addressed. Phone: 979-845-0956. Fax: 979-845-4719. E-mail: lindahl@chem.tamu.edu.

[1]Abbreviations: *ATM1* and Atm1p, gene and protein, respectively, of the ABC transporter of mitochondria 1; BPS, bathophenanthrolinedisulfonate; BVS, bond valence sum; CIA, cytosolic iron−sulfur assembly; DNPH, 2,4-dinitrophenylhydrazine; EDX, energy dispersive X-ray; EGTA, ethylene glycol bis(2-aminoethyl ether)-*N*,*N*,*N*′,*N*′-tetraacetic acid; EM, electron microscopy; EPR, electron paramagnetic resonance; EXAFS, extended X-ray absorption fine structure; Gal-ATM1, a genetic construction in which a galactose-inducible promoter replaces the natural *ATM1* promoter; Gal-ATM1/Gal/O_2, Gal-ATM1 cells grown on minimal media with galactose as a carbon source and under O_2; Gal-ATM1/Glu/O_2, same but with glucose as a carbon source; Gal-ATM1/Glu/Ar, same as Gal-ATM1/Glu/O_2 but under an argon atmosphere; HAADF, high-angle annular dark field; IM, inner mitochondrial membrane; ISC, iron−sulfur cluster; OD, optical density; PMSF, phenylmethanesulfonyl fluoride; ROS, reactive oxygen species; STEM, scanning transmission electron microscope; TEM, transmission electron microscope; WT, wild-type cells, strain W303; W303/Gal/O_2, W303 cells grown on minimal media with galactose as a carbon source and under O_2; W303/Glu/O_2, same but with glucose as a carbon source; W303/Glu/Ar, same as W303/Glu/O_2 but under an argon atmosphere; XANES, X-ray absorption near edge structure; XAS, X-ray absorption spectroscopy.

 Published on Web 09/17/2009

Fe also accumulates in mitochondria of strains in which ISC assembly components are abrogated or repressed by genetic manipulation (e.g., Yfh1p-deleted or Yah1p-depleted cells). In these cases the accumulated Fe is present as aggregated ferric nanoparticles that exhibit superparamagnetic relaxation (*10*, *11*).

The accumulation of Fe results from a shift in cellular Fe homeostasis, a partially understood process involving the Fe-sensing transcription factors Aft1p and Aft2p (*12*). Under Fe-deficient conditions, Aft1p (and presumably Aft2p) moves into the nucleus where they upregulate a group of genes known as the iron regulon. The net effect of this is to increase the rate of cellular Fe import and probably mitochondrial Fe import. Abolishing ISC assembly in mitochondria has a similar effect, causing Aft1p/Aft2p to behave as though the cytosol is Fe-deficient. Rutherford *et al.* (*13*) hypothesized that X is generated as a product of mitochondrial ISC assembly and that this signaling molecule is transferred to the cytosol via Atm1p where it is sensed by Aft1p/Aft2p. Thus, in the absence of ISC assembly, or under Atm1p-depleted conditions, the cytosol would be deficient in X, thereby causing Aft1p/Aft2p to upregulate the iron regulon.

An Atm1p homologue in *Chlamydomonas reinhardtii*, Cds1p, is upregulated when cells are exposed to Cd (*14*). This ABC half-transporter exports Cd(II) multithiol phytochelatin complexes from the mitochondrial matrix for metal detoxification. Although Fe does not accumulate in mitochondria of Cds1p-deficient cells, such cells are hypersensitive to Fe, indicating an indirect association with Fe homeostasis.

ABCB7 is the human functional orthologue of Atm1p (*15*, *16*). Patients with X-linked sideroblastic anemia with cerebellar ataxia (XLSA/A) have genetic mutations in ABCB7. In this disease, Fe accumulates in the form of ring-shaped sideroblasts, and mitochondria are loaded with iron (*17*). Heme biosynthesis and Fe regulation are also abrogated in a mouse model of this disease (*18*). Thus, understanding the function of Atm1p has considerable implications for human health.

In this study, we have examined the type of Fe that accumulates in mitochondria of Atm1p-depleted yeast cells using Mössbauer spectroscopy, electron paramagnetic resonance (EPR), electronic absorption (UV−vis) spectroscopy, X-ray absorption spectroscopy (XAS), and electron microscopy (EM). We find that the accumulated Fe is similar to that found in Yah1p-depleted (*11*) and Yfh1p-deleted (*10*) mitochondria. In contrast to previous results (*5*, *7*), we also observed a significant ISC defect in mitochondria from aerobic cells fully and partially depleted in Atm1p. There is no ISC defect in *anaerobic* Atm1p-depleted cells, confirming previous studies that Atm1p is not directly involved on ISC assembly (*7*). Collectively, these results suggest that Fe/S clusters may assemble in Atm1p-depleted mitochondria of aerobic cells but then rapidly degrade upon exposure to O_2 or ROS.

EXPERIMENTAL PROCEDURES

Yeast Strains and Media. W303 (*MAT*α, *ura3*−*1*, *ade2*−*1*, *trp1*−*1*, *his3*−*11,15*, *leu2*−*3,112*) served as the wild-type strain of *S. cerevisiae* in this study. The Gal-ATM1 strain is a derivative of W303 in which the wild-type *ATM1* promoter has been exchanged for a galactose-inducible promoter (*7*). (Both strains were generously provided by Roland Lill.) W303 cells were maintained on YPAD (standard rich medium plates containing 2% (w/v) glucose, also supplemented with 40 mg/L adenine sulfate). Gal-ATM1 cells were maintained on YPAGal (standard rich medium plates containing 2% (w/v) galactose, supplemented with 40 mg/L adenine sulfate). Typically one colony was used to inoculate liquid minimal medium supplemented with required nutrients (100 mg/L leucine, 40 mg/L adenine sulfate, 20 mg/L uracil, 20 mg/L histidine, and 50 mg/L tryptophan) and containing either 2% (w/v) glucose or galactose. To enhance the enrichment of ^{57}Fe for Mössbauer samples, a modified yeast nitrogen base (MPBio) which lacks copper and iron salts was used. Copper and iron were added back as copper sulfate (1 μM final concentration) and ^{57}Fe(III) citrate (20 μM final concentration).

Cell Growth and Harvesting. Cells were grown in a 25 L glass fermenter at 30 °C as described (*11*, *19*). For aerobic growths, research-grade O_2 was bubbled through a 3 in. coarse-grade frit immersed in the media at a rate of ∼1.5 L/min. For anaerobic growths, research-grade Ar (Botco Co.) replaced O_2, and the media were supplemented with ergosterol (Acros Organics, 20 mg/L final concentration) and Tween-80 (Acros Organics, 1.0 mL/L final concentration) dissolved in pure ethanol (1.0 mL/L final concentration). To prevent foaming, antifoam B emulsion (Sigma, 100 ppm final concentration) was added to the anaerobic media. Cells were grown for 44−48 h and harvested by centrifugation at OD(600) = 0.6−0.9, independent of carbon source or aerobicity. Anaerobic cells were harvested by first transferring them, via a peristaltic pump, to an Ar-atmosphere glovebox (*11*) where they were loaded into centrifuge bottles. Bottles were sealed, removed from the box, centrifuged, and then returned to the box where the cell paste was collected. At no time during growth or harvesting were these cells exposed to more than ∼5 ppm of O_2.

Mitochondria Isolation and Sample Preparation. Mitochondria were isolated as described (*11*, *19*, *20*). Briefly, lyticase-(Sigma) digested cells were disrupted in a Dounce homogenizer (tight fitting, 20−30 stokes). Cell debris was removed at 1500*g* for 5 min, and the mitochondria were pelleted at 12000*g* for 10 min. The crude mitochondria were loaded onto 16−22% Nycodenz (Sigma) discontinuous density gradients and centrifuged at 150000*g* for 1 h; purified mitochondria were collected at the gradient interface and will be referred to as in the "as-isolated" state. Some mitochondrial samples were treated with 2 mM sodium dithionite in a buffer containing 0.6 M sorbitol, 100 mM Tris (pH 8.5), and 1 mM EGTA. As-isolated and reduced mitochondria were packed in EPR tubes or Mössbauer cups as described (*11*) and frozen in liquid nitrogen for analysis. Mössbauer and EPR spectra were collected at Texas A&M University as described (*11*).

Western Blots. Purified mitochondria were analyzed by Western blot. Mitochondrial proteins (20 μg per lane) were separated by 12% SDS−PAGE and transferred onto polyvinylidene fluoride (PVDF) membranes (Bio-Rad). Membranes were blocked with 1% casein and incubated with an antibody against either Atm1p (*6*) or the mitochondrial outer membrane porin (Invitrogen). Blots were visualized using a Fujifilm LAS-4000 miniimaging system.

Oxyblot Assays. An oxyblot kit (Millipore) was used according to manufacturer's procedures. Isolated mitochondria were solubilized with 12% (w/v) SDS. The solution was derivatized with 2,4-dinitrophenylhydrazine (DNPH) and loaded onto a 12% SDS−PAGE gel. The primary antibody was raised against DNPH.

Preparation of Mitochondria for UV−Vis Spectroscopy. Mitochondria were solubilized in a buffer containing 50 mM Tris (pH 8.0), 100 mM NaCl, and 1% (w/v) sodium deoxycholate.

The resulting solution had a protein concentration of 5 mg/mL. Potassium ferricyanide (Acros Organics) and sodium dithionite (Sigma), at final concentrations of 12 μM each, were used respectively to oxidize and reduce cytochromes. Spectra were recorded using a 2 mm path length quartz cuvette (NSG Precision Cells, Inc.) on a Hitachi 3010 UV−vis spectrometer with a Head-On photomultiplier tube.

Enzyme Assays. Aconitase assays were performed essentially as described (*21*). Mitochondria were solubilized in a buffer containing 20 mM Tris (pH 7.4) and 0.5% (v/v) Triton X-100. Solubilized samples (20 μL) were mixed with 40 μL of 0.1 M Tris (pH 7.4), 40 μL of 0.5 M NaCl, and 80 μL of deionized H_2O in a 1 mm path length quartz cuvette. The reaction was initiated by the addition of 20 μL of 10 mM sodium *cis*-aconitate (Sigma). The consumption of aconitate was monitored by a decline of absorbance at 240 nm and quantified assuming a molar extinction coefficient of 3.6 mM^{-1} cm^{-1}. Reaction rates were calculated from the linear portion of the slopes. Activities were expressed as units per milligram of protein (1 unit is defined as 1 nmol of aconitate converted per minute).

Leu1p assays were performed essentially as described (*22*). Cells were grown on minimal medium (leucine concentration was lowered to 30 mg/L to increase expression of *leu1p*) and harvested when OD(600) reached ~0.7. The pellet obtained by centrifuging 30 mL of cell culture was washed with ice-cold deionized water and resuspended in 0.3 mL of lysis buffer (20 mM KH_2PO_4 buffer, pH 7.2, 50 mM NaCl, 1 mM EDTA, 0.5 mM PMSF). Approximately 0.3 mL of glass beads (Biospec Inc.; 0.5 mm diameter) was added. The mixture was vortexed for 30 s followed by 30 s on ice. This cycle was repeated five to six times. Unbroken cells and glass beads were removed by centrifugation at 10000*g* for 5 min. Immediately thereafter, 50 μL of the supernatant cell extract was mixed with 50 μL of 0.2 M KH_2PO_4 (pH 7.0) buffer, 395 μL of deionized water, and 5 μL of 0.1 M sodium citraconate (Sigma). The decline in absorbance at 235 nm was monitored for 3 min. Activity was expressed as units per milligram of protein (1 unit is defined as 1 nmol of citraconate converted per minute).

Succinate dehydrogenase assays were performed following the published procedure (*23*). The reduction of iodonitrotetrazolium chloride (INT, Sigma) to form INT-formazan was monitored at 500 nm, and the activity was expressed as units per milligram of protein (1 unit is defined as 1 nmol of INT-formazan formed per minute).

Protein and Iron Content Analysis. Mitochondrial protein concentrations were determined using the Bradford protein assay kit (Pierce) or BCA protein assay kit (Pierce) following the manufacturer's instructions. Unless otherwise noted, reported concentrations refer to packed mitochondria conditions (*19*), not adjusted for buffer void volume. Mitochondrial total iron concentrations were measured by the method of Tamarit *et al.* (*24*) but modified as follows. Packed mitochondria were diluted in 2−3 volumes of water, and 50 or 100 μL suspensions were digested in 500 μL of 30% trace-metal grade nitric acid (Fisher Scientific) at 95−100 °C overnight. Digested samples (100 μL) were mixed with 200 μL of 6.4 M ammonium acetate (Sigma), 100 μL of 0.2 M sodium ascorbate (Acros Organics), 100 μL of 10 mM bathophenanthrolinesulfonate (BPS; Sigma), and 500 μL of deionized H_2O. The concentration of $Fe(BPS)_3$ was determined from the absorbance at 535 nm assuming a molar extinction coefficient of 22167 M^{-1} cm^{-1}.

Electron Microscopy. Specimens were prepared as described (*11*). Elemental analysis was performed on a TECNAI F20 (scanning) transmission electron microscope (TEM/STEM) fitted with a Schottky field emission gun, a high-angle annular dark field (HAADF) detector, and an Oxford instruments ultrathin window energy dispersive X-ray spectroscopy (EDX) detector. The EDX spectrum in the area of interest was collected at a 200 kV accelerating voltage at an ~15° tilt angle with a stationary electron probe in STEM mode. A few EDX spectra were acquired to determine conditions that maximized the signal-to-noise ratio and simultaneously minimized sample damage. Using these conditions, X-ray spectral images were collected from the area of interest. Spatial drift was corrected by referencing a high-contrast object around the area. By choosing a proper energy window for each element, an elemental map was extracted from spectral images.

X-ray Absorption Spectroscopy. Fluorescence excitation Fe K-edge XAS data were collected directly from packed mitochondria in Mössbauer cups, held inside our standard liquid He continuous flow cryostat with a custom-designed sample holder. Data were collected on beamline 9-3 of the Stanford Synchrotron Radiation Lightsource with SPEAR3 running at 3.0 GeV and 80−100 mA beam current. Harmonic rejection was achieved by the focusing mirror being configured to a nominal 10 keV cutoff. We used a 30-element intrinsic Ge solid-state detector and Z-1 fluorescence filter with Soller slits to record the XAS fluorescence signal from samples. XAS data reduction was carried out using the EXAFSPAK program (http://www-ssrl.slac.stanford.edu/exafspak.html). The photon energy was calibrated using an internal Fe foil with the first inflection point at 7111.2 eV; E_0 was defined as 7120 eV. The Atm1p data set was the average of seven individual sweeps, each of 21 min duration. Preedge subtraction used a Gaussain model, and the EXAFS were extracted using a spline with three regions, each of polynomical order 4. Curve fitting was performed using the theoretical phase and amplitude functions calculated by FEFF 8.0 (*25*).

Mössbauer and EPR Spectroscopy. Mössbauer spectra were collected on a Model MS4 WRC spectrometer (SEE Co., Edina, MN) and were calibrated using an α-Fe foil as described (*11*). EPR spectra were collected on an X-band EMX spectrometer (Bruker Biospin, Billerica, MA) as described (*11*).

RESULTS

W303 and Gal-ATM1 Cells Grown under Different Carbon Sources. This study involved *S. cerevisiae* strains W303 and Gal-ATM1. W303 is a wild-type (WT) strain while Gal-ATM1 is a derivative of W303 in which the natural promoter for *ATM1* has been replaced by a truncated galactose-inducible promoter. The latter strain expresses Atm1p when grown on galactose but not when grown on glucose. Most batches of cells were grown with O_2 bubbled through the media, but some were bubbled with argon. Atm1p should express in W303 cells grown aerobically or anaerobically on glucose (W303/Glu/O_2 and W303/Glu/Ar) and grown aerobically on galactose (W303/Gal/O_2). Atm1p should also express in Gal-ATM1 cells grown aerobically on galactose (Gal-ATM1/Gal/O_2), but it should not express in Gal-ATM1 cells grown on glucose, regardless of whether growing cells are bubbled with O_2 (Gal-ATM1/Glu/O_2) or argon (Gal-ATM1/Glu/Ar).

Consistent with this, Atm1p in our samples was virtually undetectable by Western blot analysis of mitochondrial extracts of Gal-ATM1/Glu/O_2 cells (Figure 1, lane 4), while it was readily detected in extracts of W303/Gal/O_2 (lane 1), W303/Glu/O_2

(lane 2), and Gal-ATM1/Gal/O_2 cells (lane 3). When normalized to the density of the porin control (Figure 1, bottom panel), the Atm1p expression level in Gal-ATM1/Gal/O_2 cells was calculated to be 45 ± 5% of that in W303/Gal/O_2 cells. Thus, in cells grown on minimal medium containing galactose, the Atm1p expression level was lower when the truncated galactose-inducible promoter was used. A similar result has been observed previously (*7*). This had some biophysical consequences (see below).

Purified mitochondria from Gal-ATM1/Glu/O_2 cells contained 14 times higher levels of iron than mitochondria from W303/Glu/O_2 cells (Table 1). The Fe concentration in Gal-ATM1/Gal/O_2 cells ([Fe] ~ 2 mM, estimated from Mössbauer intensity, as described (*19*)) was intermediate. The accumulation of Fe in Atm1p-depleted and partially depleted mitochondria suggests that under these conditions the import flux of Fe into the organelle had increased.

The protein concentration of mitochondria (milligrams of protein per milliliter of packed mitochondria) from Gal-ATM1/Glu/O_2 cells, determined by the Bradford method, was lower than that from W303/Glu/O_2 cells (Table 1). To assess whether this lower than expected value arose from interference from Fe(III) nanoparticles (see below), we quantified proteins by the BCA method (Pierce); however, no difference relative to the WT value was observed. The difference in protein concentration may be real, perhaps resulting from the repression of respiration/citric acid cycle proteins (*5*).

The Fe concentration of packed mitochondria isolated from Gal-ATM1 cells grown under anaerobic conditions was similar to that of anaerobically grown WT cells, and both were lower than in aerobic WT mitochondria (Table 1). The protein concentration of anaerobic mitochondria was also low, about 50% of that isolated from aerobically grown WT cells. There are significant differences between anaerobic *vs* aerobic mitochondria. Although the morphology of both is similar (*26*), the concentration of many proteins, including Fe-containing proteins such as the respiratory complexes and particular citric acid cycle enzymes, is significantly reduced in anaerobic mitochondria (*27*). This may result in the lower Fe and protein concentrations observed. Alternatively, anaerobic mitochondria may simply not pack as tightly as aerobic mitochondria, perhaps due to differences in lipid composition (*28*). These differences do not appear to have affected the density of the anaerobic organelles, as they were purified using the same Nycodenz gradients as mitochondria from aerobically grown cells. The lower Fe concentration indicated that Fe did not hyperaccumulate in mitochondria from Atm1p-depleted cells grown under anaerobic conditions.

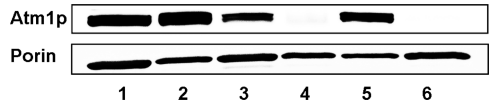

FIGURE 1: Western blots of Atm1p and porin in isolated mitochondria: lane 1, W303/Gal/O_2; lane 2, W303/Glu/O_2; lane 3, Gal-ATM1/Gal/O_2; lane 4, Gal-ATM1/Glu/O_2; lane 5, W303/Glu/Ar; lane 6, Gal-ATM1/Glu/Ar. Top panel: Blot treated with anti-Atm1p antibody. Bottom panel: Blot treated with an antibody for the mitochondrial outer membrane protein porin which served as a loading control.

Ferric Phosphate Nanoparticles in Atm1p-Depleted Mitochondria. The 4.5 K low-field Mössbauer spectra of Atm1p-depleted mitochondria (Figure 2A) exhibited an intense quadrupole doublet with isomer shift $\delta = 0.53$ mm/s, quadrupole splitting $\Delta E_Q = 0.73$ mm/s, and line width $\Gamma = 0.68$ mm/s. These parameters are similar to those of the doublet exhibited by ferric nanoparticles in Yah1p-depleted cells ($\delta = 0.52$ mm/s, $\Delta E_Q = 0.63$ mm/s, and $\Gamma = 0.55$ mm/s) (*11*). A high-field spectrum of Atm1p-depleted mitochondria (Figure 2B) was also similar to that of Yah1p-depleted mitochondria.

Atm1p-depleted mitochondria exhibited a very broad EPR signal centered at $g \sim 2.0$ and with inverse Curie law behavior (Figure 3, top panel), similar to that exhibited by Yah1p-depleted mitochondria (*11*). Such signals indicate superparamagnetic relaxation, consistent with the aggregation of ferric nanoparticles. The superparamagnetic EPR signal from Atm1p-depleted mitochondria was ~1.7-fold broader than that from Yah1p-depleted mitochondria, which might indicate subtle differences in size, composition, and/or microcrystallinity of the nanoparticles. The only other EPR signal evident in the spectra is a minor feature at $g = 4.3$ due to a small amount of rhombic high-spin Fe(III) and an isotropic signal at $g \sim 2.00$ probably due to organic-based radicals.

Atm1p-depleted mitochondria were investigated by analytical electron microscopy. In STEM-HAADF micrographs (Figure 4), Fe species within Gal-ATM1/Glu/O_2 mitochondria appear brighter than background. Brightness in these images depends on the relative concentration and atomic number (Z) of contributing atoms. High magnification STEM images (Figure 4, panels on left) revealed bright spheres indicating high Z elements such as iron. Elemental maps (panels on right) reveal that those areas are rich in both iron and phosphorus, with a molar {Fe:P} ratio of {0.7:1.0} (relative uncertainty ~10%). These particles are also associated with oxygen but not with carbon (Figure 4) or sulfur or nitrogen (data not shown). Close-up images (Figure 4, bottom left panel) suggest 2−4 nm diameters for these ferric phosphate nanoparticles.

X-ray absorption spectroscopy (XAS) was used to further characterize the ferric nanoparticles in mitochondria from Atm1p-depleted cells. The XANES region (Figure 5a) was typical of Fe(III) ions coordinated by O/N donor ligands but was not typical of Fe−S centers. Neither tetrahedral nor square-planar geometries appear likely, but various 5-coordinate or distorted

Table 1: Fe and Protein Concentrations in Packed Mitochondria and Activities in Isolated Mitochondrial Suspensions[a]

	W303/Glu/O_2	Gal-ATM1/Glu/O_2	W303/Glu/Ar	Gal-ATM1/Glu/Ar
[Fe] (μM)	630 ± 40	8900 ± 400	170 ± 10	180 ± 10
[protein] (mg/mL)	57 ± 5	26 ± 3	31 ± 4	34 ± 5
aconitase activity (units/mg of protein)	670	80	650	700
succinate dehydrogenase activity (units/mg of protein)	14	5	not determined	not determined
Leu1p activity (units/mg of protein)	150	ND[b]	320	ND[b]

[a]The error for activity assays is estimated at 20%. [b]ND, activity not detectable (lower than 20 units/mg of protein).

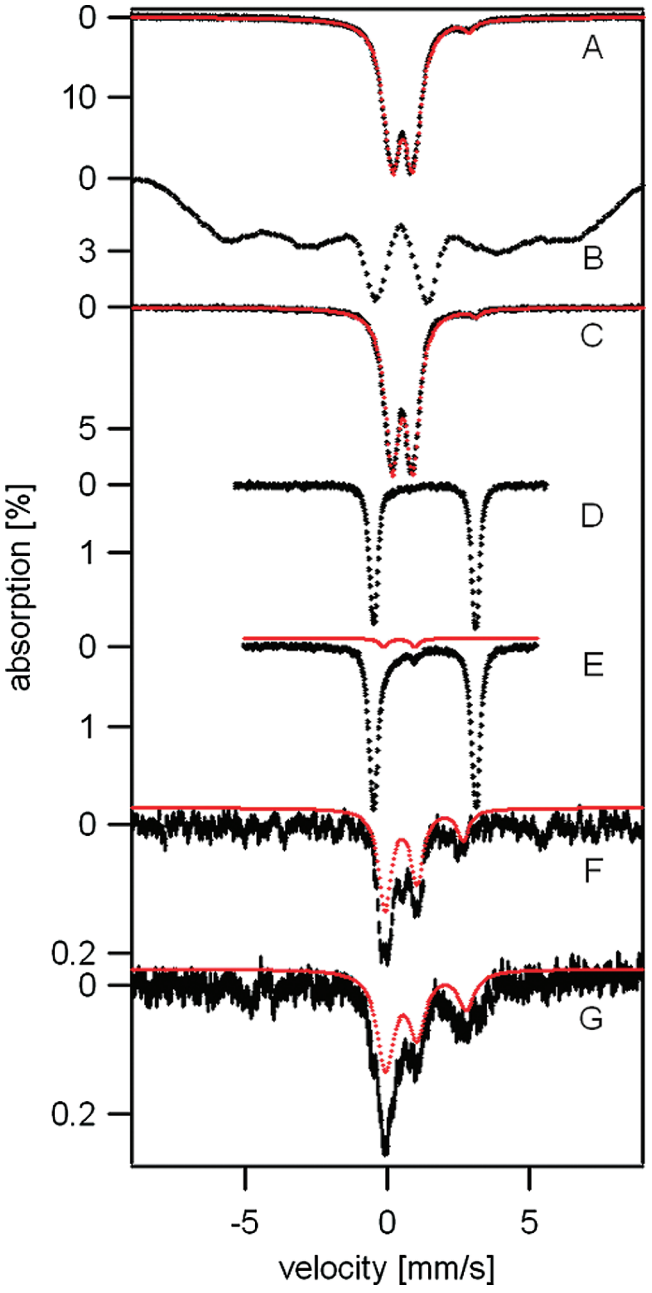

FIGURE 2: 4.5 K Mössbauer spectra of mitochondria from Gal-ATM1 and W303 cells. (A) Gal-ATM1/Glu/O_2, collected with 40 mT field applied parallel to γ-rays (low applied field). The solid red line is the sum of the Fe(III) nanoparticle doublet and a HS Fe(II) doublet. (B) Same as (A) but with 8 T applied field. (C) Gal-ATM1/Gal/O_2, low applied field. The solid red line is the sum of the Fe(III) nanoparticle doublet and a HS Fe(II) doublet. (D) Same as (A) but reduced with sodium dithionite. (E) Same as (C) but reduced with sodium dithionite. The solid line above the data outlines a $[Fe_4S_4]^{2+}$ doublet (δ = 0.45 mm/s, ΔE_Q = 1.15 mm/s). (F) W303/Glu/Ar, low applied field. The solid line above the data outlines the sum of two major doublets ($[Fe_4S_4]^{2+}$ and HS Fe(II)), representing ~70% of Fe. (G) Gal-ATM1/Glu/Ar, low applied field. The solid line above the data outlines the sum of the same two major doublets, representing ~80% of Fe.

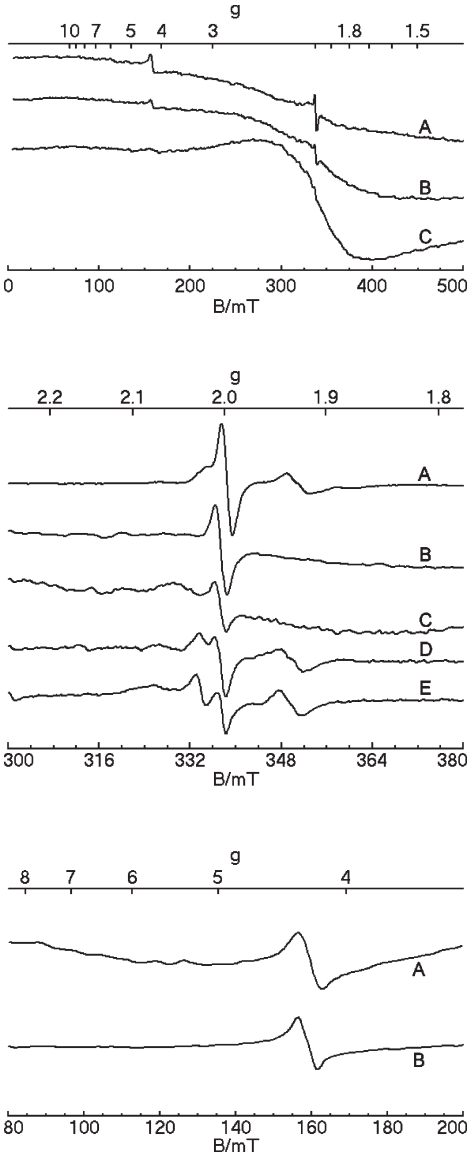

FIGURE 3: X-band EPR spectra of isolated mitochondria from Gal-ATM1 and W303 cells. Top panel: From Gal-ATM1/Glu/O_2 cells. A, 10 K; B, 30 K; C, 80 K; microwave frequency for all spectra, 9.46 GHz; microwave power for A, B, and C, 20 mW. Middle panel: g = 2 region. A, W303/Gal/O_2; B, Gal-ATM1/Glu/O_2; C, same as B but reduced with sodium dithionite; D, W303/Glu/Ar; E, Gal-ATM1/Glu/Ar. Temperature, 10 K; microwave power, 0.2 mW. Bottom panel: g = 4−6 region. A, as-isolated Gal-ATM1/Glu/O_2 mitochondria; B, same as A but treated with sodium dithionite. Temperature, 10 K; microwave power, 20 mW.

6-coordinate geometries are possible. The 1s → 3d transition on the edge was more intense than expected for a perfect octahedron. The assumption of 5-coordinate Fe−O gave a slightly better BVS than when 6-coordination was assumed. The corresponding background-subtracted EXAFS data (Figure 5c) are of high quality, extending to $k \sim 16$ Å^{-1}. The Fourier transform of these data (Figure 5b) exhibited a single first-shell peak from oxygen and/or nitrogen backscatterers at an average distance of 1.97 Å as well as a clear outer shell FT peak at 3.21 Å. Results of fits to various models are shown in Table 2 (plots comparing EXAFS and FTs of all fits are provided in Supporting Information). The long-distance backscatterer fitted well to P but not to Fe. The fit assuming a single second-shell P from a phosphate ion bound to Fe yielded an Fe−P Debye−Waller factor that was too small to be physically meaningful, whereas the fit assuming two phosphate groups (Figure 5b,c, red solid lines) yielded a Debye−Waller factor that is larger and physically reasonable (Table 2). Thus, this latter fit was preferred, though we cannot exclude a mixture of Fe sites with one and two phosphate ligands, an environment expected for nanoparticles where there are both interior and surface Fe sites.

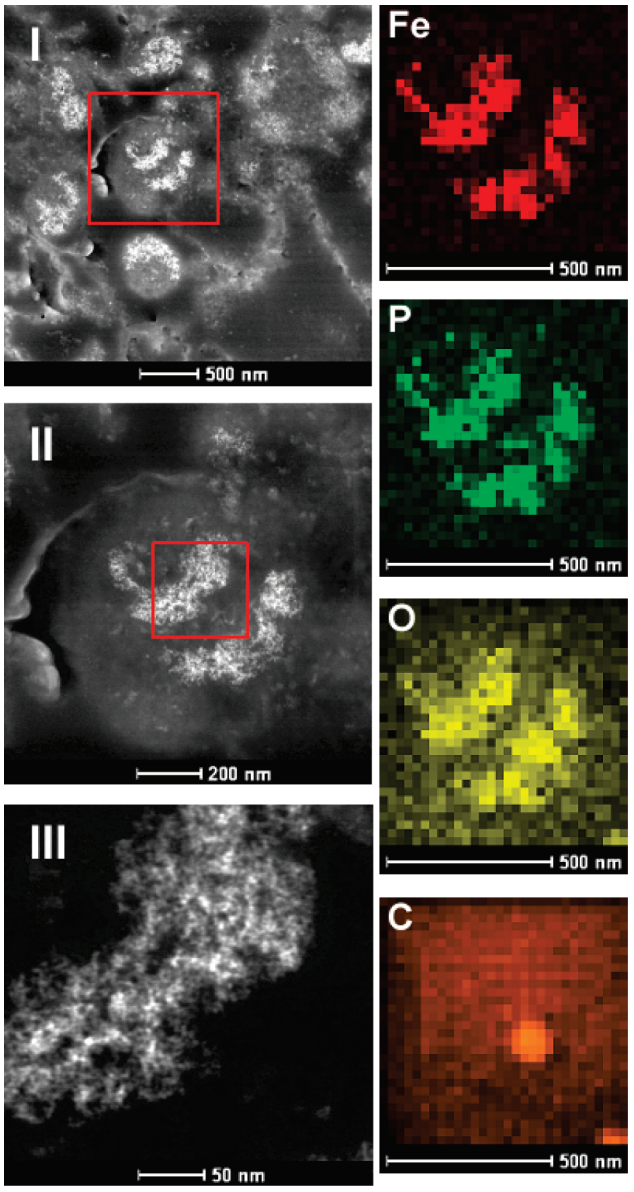

FIGURE 4: STEM-HAADF images and elemental maps of iron deposits in mitochondria isolated from Gal-ATM1/Glu/O_2 cells. Images I, II, and II were obtained at increasing magnification, with the red box in each panel corresponding approximately to the full image in the next lower panel. The red box in image I also corresponds to the region scanned for Fe, P, O, and C maps. The bright spot near the center of the carbon map is probably a beam-damaged mark.

Characterization of Iron in Gal-ATM1/Gal/O_2 Mitochondria. We initially expected that mitochondria from Gal-ATM1 cells grown on galactose/O_2 would serve as a control in which Atm1p would be expressed at WT levels. However, Western blot analysis revealed that Atm1p concentrations were reduced (Figure 1, compare lanes 1 and 3). Interestingly, the extent of reduction appears to have been sufficient to alter the phenotype of the strain. Mössbauer spectra of as-isolated Gal-ATM1/Gal/O_2 mitochondria were typical of ferric nanoparticles (Figure 2C). Mössbauer parameters for the nanoparticle doublet was similar to that of Gal-ATM1/Glu/O_2 mitochondria (δ = 0.52 mm/s, ΔE_Q = 0.73 mm/s) except for a lower percentage effect which was consistent with a lower Fe concentration in these organelles.

These results illustrate the effect of reducing but not fully depleting Atm1p levels in cells. The qualitative (but less severe)

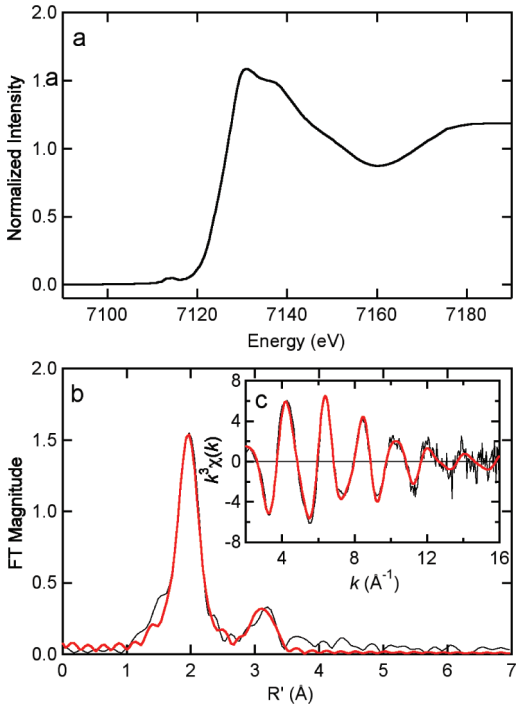

FIGURE 5: X-ray absorption spectra of mitochondria isolated from Gal-ATM1/Glu/O_2 cells: (a) XANES; (b) FT (k = 2.0−16.0 Å^{-1}, k^3 weighting); (c) EXAFS. Solid red lines are simulations assuming the FeO_5P_2 model of Table 1.

Table 2: Curve Fitting Results for Fe K-Edge EXAFS[a,c]

sample filename (k range), $\Delta k^3\chi$	fit	shell	R_{as} (Å)	σ_{as}^2 (Å^2)	ΔE_0 (eV)	f' [b]
FMG0B (2−16 Å^{-1}), 12.6477	1	Fe−O_5	1.973	0.0055	−2.92	0.070
	2	Fe−O_5	1.973	0.0055	−2.92	0.058
		Fe−P_1	3.210	0.0025	[−2.92]	
	3	Fe−O_5	1.973	0.0055	−2.84	0.057
		Fe−P_2	3.210	0.0067	[−2.84]	
	4	Fe−O_5	1.973	0.0055	−2.80	0.063
		Fe−Fe_1	3.020	0.0105	[−2.80]	
	5	Fe−O_5	1.974	0.0055	−2.74	0.062
		Fe−Fe_2	3.003	0.0163	[−2.74]	

[a]Shell is the chemical unit defined for the multiple scattering calculation. Subscripts denote the number of scatterers per metal. R_{as} is the metal-scatterer distance. σ_{as}^2 is a mean square deviation in R_{as}. ΔE_0 is the shift in E_0 for the theoretical scattering functions. [b]f' is a normalized error (chi-squared): $f' = \{\sum_i [k_3(\chi_i^{obs} - \chi_i^{calc})]^2/N\}^{1/2}/[(k^3\chi^{obs})_{max} - (k^3\chi^{obs})_{min}]$. [c]BVS = $\sum\exp[(r_0 - r)/B]$, B = 0.37, r_0(Fe(III)−O) = 1.759 (*47*). A chemically reasonable set of distances should yield a BVS value close to the expected valence (3.00 in this case). For all five fits shown in the table, BVS = 2.80. [d]Numbers in square brackets were constrained either to be a multiple of the above value (σ_{as}^2) or to maintain a constant difference from the above value (R_{as}, ΔE_0).

development of the same phenotype as observed for mitochondria that were fully depleted in Atm1p suggests that there is *not* a large functional excess of Atm1p in WT mitochondria from cells grown on minimal media. Had Atm1p been present in excess in WT cells, a 2.5-fold decline of concentration would probably not have caused the observed phenotype. In the following studies WT (W303) cells grown under the same condition served as a control.

Atm1p-Depleted Mitochondria from Gal-ATM1/Glu/O_2 Cells Have Reduced Levels of Fe/S Clusters. Mössbauer spectra of Gal-ATM1/Glu/O_2 mitochondria (Figure 2A,B) did

not include features typical of $S = 0$ $[Fe_4S_4]^{2+}$ clusters; such features dominate spectra of WT mitochondria (*19*). To explore whether any such clusters were "hiding" underneath the broad doublet due to ferric nanoparticles, we treated Gal-ATM1/Glu/O_2 mitochondria with dithionite. The resulting Mössbauer spectrum (Figure 2D) was dominated by a quadrupole doublet due to high-spin Fe(II) ions. Our analysis suggests that no more than ~2% of spectral intensity could reflect $S = 0$ $[Fe_4S_4]^{2+}$ clusters. In WT samples, about half of the Fe in mitochondria arises from such clusters (*19*). The spectral intensity for the reduced sample was lower than for the as-isolated sample, suggesting that about two-thirds of the Fe had been exported from the mitochondria as a result of dithionite treatment. A similar phenomenon was observed upon reduction of Yah1p-depleted mitochondria (*11*). Assuming an [Fe] of ~3 mM, a 2% spectral intensity would correspond to 60 μM Fe. This would represent an ~7-fold reduction of $[Fe_4S_4]$ clusters relative to WT levels.

Analysis of the Gal-ATM1/Gal/O_2 sample allowed another estimate of $[Fe_4S_4]$ cluster levels. After treatment with dithionite, the Gal-ATM1/Gal/O_2 sample (that yielded the spectrum of Figure 2C) exhibited the spectrum of Figure 2E; it was again dominated (~90% of spectral intensity) by a HS Fe(II) doublet. A small feature, representing ca. 5% of spectral intensity, was simulated as a quadrupole doublet due to $[Fe_4S_4]^{2+}$ clusters. We regard this as an upper limit. Assuming an [Fe] of 2 mM for this sample, 5% would correspond to 100 μM Fe, suggesting an ~4-fold reduction of $S = 0$ $[Fe_4S_4]^{2+}$ clusters relative to WT mitochondria.

EPR spectroscopy is better suited to observe Fe/S clusters in their reduced state, and so Atm1p-depleted mitochondria were transferred from Mössbauer to EPR holders (while maintaining them at LN_2 temperature). The resulting EPR spectra (Figure 3, middle panel, trace B for the as-isolated sample and trace C for dithionite-reduced sample) were virtually devoid of $g_{av} = 1.94$ or 1.90 signals. These signals were present in spectra of WT mitochondria (Figure 3, middle panel, trace A), and they probably arise from the $S = {}^1/_2$ $[Fe_2S_2]^{1+}$ clusters of succinate dehydrogenase and the Rieske Fe/S protein (*19*). Low-field spectra of both as-isolated and dithionite-reduced Gal-ATM1/Glu/O_2 mitochondria samples did not exhibit features at $g = 4-6$ which typify $S = {}^3/_2$ $[Fe_4S_4]^{1+}$ clusters (Figure 3, bottom panel).

Previous conclusions that Atm1p-depleted mitochondria contain WT concentrations of Fe/S clusters were based largely on the presence of substantial aconitase activities in Atm1p-depleted cell extracts and on ^{55}Fe incorporation into mitochondrial Fe/S proteins (*6*, *7*). Using WT and *atm1*Δ strains grown on yeast extract−peptone medium containing 2% galactose, Kispal *et al.* reported that the aconitase activity of *atm1*Δ mitochondria was ~40% of WT levels (*6*). When the Gal-ATM1 strain was grown on lactate to deplete Atm1p, the aconitase activity in mitochondria was ~70% of WT levels (*7*). The same assay performed on our samples revealed reduced (but still nonzero) activities. The aconitase activity of a Gal-ATM1 mitochondrial extract was ~12% of the WT level in mitochondrial extracts (for cells grown on glucose in minimal media) (Table 1). In extracts of mitochondria isolated from galactose-grown cells, aconitase levels (900 units/mg) were 64% of WT levels (1400 units/mg). Thus, there was an effect of growth media, carbon source, and/or the extent of Atm1p depletion on mitochondrial Fe/S levels and therefore on aconitase activities. Succinate dehydrogenase activities showed a similar pattern (Table 1).

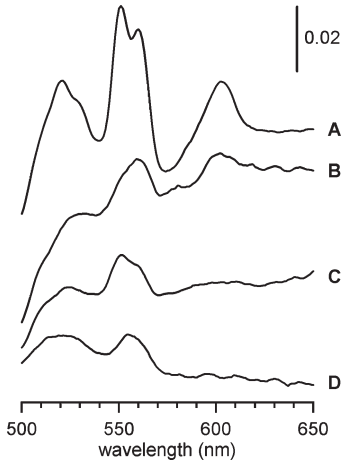

FIGURE 6: Electronic absorption reduced-minus-oxidized difference spectra of mitochondria isolated from W303 and Gal-ATM1 cells. Spectra were obtained at room temperature from samples treated with sodium dithionite. They were subtracted from those obtained from samples treated with ferricyanide. A, W303/Glu/O_2; B, Gal-ATM1/Glu/O_2; C, from W303/Glu/Ar; D, Gal-ATM1/Glu/Ar.

These activities imply significantly reduced levels of Fe/S clusters in mitochondria that are *fully* depleted in Atm1p and moderately reduced levels of Fe/S clusters under conditions of *partial* depletion. They are consistent with our biophysical results but are perhaps somewhat higher than indicated by them. One possible explanation is that Fe/S clusters are inserted preferentially into apoaconitase (or aposuccinate dehydrogenase) molecules, such that this activity overestimates the total level of mitochondrial Fe/S clusters. Also apparent is that there is a relationship between aconitase activity and the extent of Atm1p depletion, which in turn depends sensitively on media and growth conditions. Our results are generally consistent with those of Kispal *et al.* in that they also observed lower aconitase activities in Atm1p-depleted and *atm1*Δ strains (*6*, *7*), relative to WT levels. However, based on the moderate decline in activity of mitochondrial Fe/S proteins observed for Atm1p-depleted cells relative to the loss of extramitochondrial Fe/S proteins, Kispal *et al.* (*6*, *7*) concluded that neither depleting nor deleting cells of *ATM1* had any significant effect on the function of Fe/S proteins inside the organelle. The more significant decline observed here along with our biophysical data indicates that the level of ISC assembly in Atm1p-depleted mitochondria is *reduced substantially* relative to WT, by a factor of 4−8.

Atm1p-Depleted Mitochondria from Gal-ATM1/Glu/O_2 Cells Are Deficient in Hemes. Previous studies have reported that Atm1p-depleted cells have either WT levels or reduced levels of heme centers, depending on growth media (*5*). To evaluate this in our Atm1p-depleted mitochondria, samples were examined by electronic absorption spectroscopy. Difference spectra (Figure 6) revealed that heme $a + a_3$, b, and $c + c_1$ concentrations were each ~6-fold lower in Gal-ATM1/glucose/O_2 mitochondria relative to those in WT mitochondria grown on the same carbon source. This decrease in heme concentrations is roughly similar to that observed in overall ISC concentrations.

Atm1p-Depleted Mitochondria Accumulate High-Spin (HS) Fe(II) Ions. Besides the dominant Fe(III) nanoparticle doublet, the low-field 4.5 K Mössbauer spectrum of Atm1p-depleted mitochondria from Gal-ATM1/Glu/O_2 cells exhibited a quadrupole doublet typical of high-spin Fe(II) ions (Figure 2A and close-up in Figure 7A). The Mössbauer parameters asso-

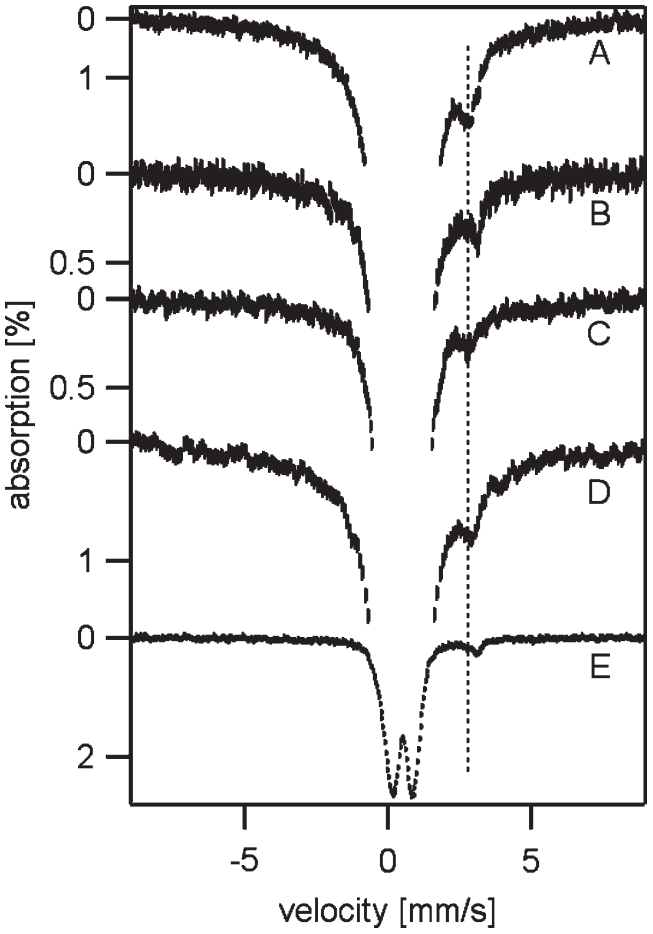

FIGURE 7: Mössbauer spectra showing high-spin Fe(II) species in Atm1p-depleted and Yah1p-depleted mitochondria and whole cells. All spectra were collected 4.5 K with 40 mT parallel applied field. A, Gal-ATM1/Glu/O_2 mitochondria; B, Gal-ATM1/Gal/O_2 mitochondria; C, Gal-ATM1/Glu/O_2 cells; D, mitochondria from Yah1p-depleted cells grown on glucose/O_2 (batch 1); E, same as B but a different batch harvested after 35 h of growth. A vertical dashed line is drawn at 2.75 mm/s.

ciated with this doublet could not be determined accurately since the low-energy line was buried in the nanoparticle doublet. The high-energy line was located at 2.75 ± 0.02 mm/s (average of three batches), which is different from the high-energy line of hexaqua high-spin Fe(II) ions in phosphate buffer at pH 7.4 (2.9 mm/s) (Supporting Information of ref *11*). The line width of the doublet was quite broad ($\Gamma \sim 1$ mm/s), suggesting multiple species. The doublet corresponded to 3−5% of spectral intensity, which may seem insignificant. However, assuming ~10 mM total [Fe] for this sample, the concentration of HS Fe(II) ions in these nanoparticle-packed mitochondria would correspond to 300−500 μM, roughly half of the total Fe concentration in WT mitochondria!

A similar HS Fe(II) doublet was present in spectra of mitochondria from Gal-ATM1/Gal/O_2 cells (Figures 2C and 7B). In this case, the high-energy line was at 3.08 ± 0.02 mm/s (average of two batches), which is slightly different from that for glucose-grown mitochondria and the HS Fe(II) high-energy line of hexaqua Fe(II) ions. Also, the line width ($\Gamma \sim 0.5$ mm/s) of the high-energy line in spectra of Gal-ATM1/Gal/O_2 mitochondria was substantially narrower than that for glucose-grown cells, suggesting that fewer species contribute.

The overall spectral intensity in a batch of mitochondria from Gal-ATM1/Gal/O_2 cells that were harvested after 35 h of growth

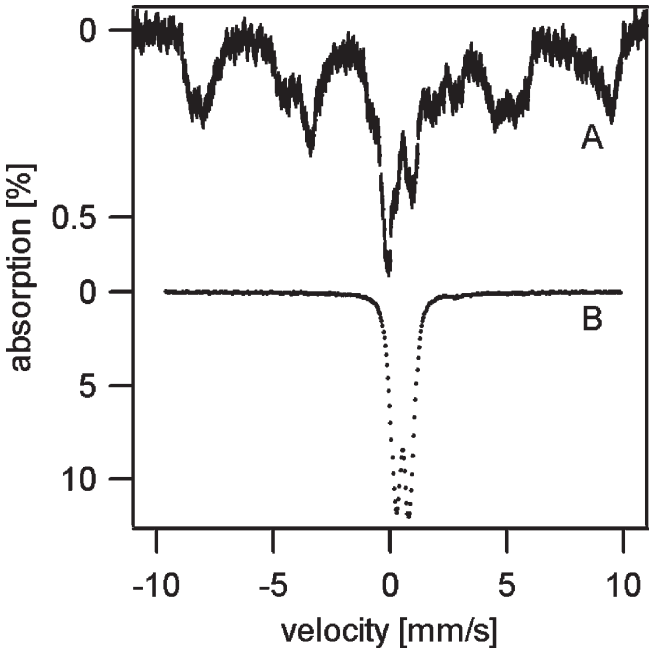

FIGURE 8: 4.5 K Mössbauer spectra of whole yeast cells. A, W303/Glu/O_2; B, Gal-ATM1/Glu/O_2. A 40 mT parallel field was applied.

on minimal galactose-containing medium was ~2.5% effect (Figure 7E) while that for a batch harvested 45 h after inoculation was ~6% effect (Figure 2C). The difference in percent effect suggests that the *extent of nanoparticle accumulation increases with growth time*. The spectral intensity of the HS Fe(II) doublet *decreased* (4% for the 35 h batch and 2% for the 45 h batch), but the estimated concentrations of HS Fe(II) in the mitochondria were essentially invariant (~50 μM in each case).

No HS Fe(II) doublet was reported in a Mössbauer spectrum of mitochondria isolated from Yah1p-depleted mitochondria (*11*) even though these organelles also contained ferric phosphate nanoparticles. However, careful reinspection of the published spectrum revealed the possibility of such a species, and spectra from two other batches of Yah1p-depleted mitochondria (Figure 7D and another not shown) confirmed that these mitochondria also contain substantial amounts of HS Fe(II) ions. In these spectra, the intensity of the Fe(II) doublet represented ~5% of the intensity, similar to that for Atm1p-depleted mitochondria. Assuming 7.4 mM Fe (*11*), this corresponds to ~150 μM, which is again a substantial concentration. Analogous inspection of the published Mössbauer spectrum of Yfh1-depleted mitochondria (*10*) failed to reveal any evidence for this doublet.

Cellular Accumulation and Redistribution of Iron in Atm1p-Depleted Mitochondria. By growing wild-type yeast cells on minimal media enriched in ^{57}Fe, we were able to obtain *whole cell* Mössbauer spectra (Figure 8A). High-spin Fe(III) species from an unknown but nonmitochondrial location in the cell dominated the spectrum, while a quadrupole doublet with parameters typical of $[Fe_4S_4]^{2+}$ clusters was also evident. Thus, our first glimpse of the iron-ome of a fermenting yeast cell reveals that the vast majority of its Fe is present as mononuclear Fe(III) complexes.

The corresponding 4.5 K Mössbauer spectrum of whole Gal-ATM1/Glu/O_2 cells (Figure 8B) is dramatically different in three major respects. First, the Fe concentration was higher by a factor of 10. Second, most of that Fe appeared to be in the form of ferric nanoparticles. Third, the high-spin mononuclear Fe(III) species

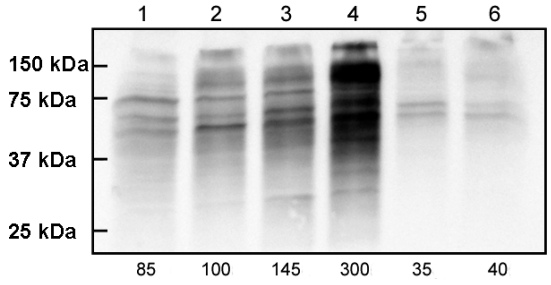

FIGURE 9: Oxyblot analysis of mitochondria isolated from W303 and Gal-ATM1 cells: lane 1, W303/Gal/O_2; lane 2, W303/Glu/O_2; lane 3, Gal-ATM1/Gal/O_2; lane 4, Gal-ATM1/Glu/O_2; lane 5, W303/Glu/Ar; lane 6, Gal-ATM1/Glu/Ar. The total level of carbonylated proteins was calculated from each lane, normalized relative to the intensity in lane 2, and shown as a percentage of that at the bottom of the figure.

observed in WT cells was absent (see Figure 7C for close-up). Also present at the level of ~2% of cellular Fe were high-spin Fe(II) ions, as evidenced in a close-up of the baseline (Figure 7C). The central doublet typical of Fe/S clusters was also not observed in spectra of Atm1p-depleted whole cells. A small contribution of such clusters could have been present but undetectable due to the dominance of the nanoparticle doublet.

Anaerobic Growth of Atm1p-Depleted Cells. In a previous study, we found that mitochondria of Yah1p-depleted cells did not accumulate Fe when such cells were grown anaerobically (with Ar rather than O_2) on glucose (*11*). A similar experiment was carried out using Gal-ATM1/Glu/O_2 cells. The resulting 4.5 K low-field Mössbauer spectrum (Figure 2G) was dominated by two doublets. One accounted for ~30% of spectral intensity and was due to high-spin Fe(II) ions ($\delta \sim 1.3$ mm/s, $\Delta E_Q = 2.8$ mm/s). The other doublet, representing ~50% of spectral intensity, possessed parameters typical of $[Fe_4S_4]^{2+}$ clusters. The percent effect was quite low, indicating no hyperaccumulation of Fe or evidence of ferric nanoparticles. The spectrum of WT cells grown under anaerobic conditions was similar (Figure 2F). UV−vis spectra of these mitochondria revealed low concentrations of heme centers (Figure 6C,D), The diminished level of hemes relative to that in aerobic cells probably reflects the O_2 dependence of heme biosynthesis (*29*). Hemes $a + a_3$ were essentially absent, probably due to a direct requirement of O_2 for heme *a* synthesis (*30*).

Aconitase activities in mitochondria isolated from anaerobic W303/Glu/O_2 and Gal-ATM1/Glu/O_2 cells were also determined. The results (Table 1) showed high activities in both strains, indicating the presence of mitochondrial Fe/S clusters. Leu1p is a cytosolic Fe/S-containing enzyme, and its activity was measured to assess the functioning of the CIA machinery. The results (Table 1) show the absence of Leu1p activity in Gal-ATM1/Glu cells grown under either aerobic or anaerobic conditions.

Oxidative Stress Levels in Atm1p-Depleted Mitochondria. Using the oxyblot assay, we examined the level of oxidative stress associated with mitochondria isolated from Gal-ATM1 cells. Relative to the degree of oxidative stress associated with mitochondria from W303/Gal/O_2 and W303/Glu/O_2 cells (Figure 9, lanes 1 and 2), mitochondria from Gal-ATM1 cells grown on galactose/O_2 (lane 3) and glucose/O_2 (lane 4) exhibited greater levels of oxidative stress, consistent with previous findings (*6*). The extent of oxidative damage was especially severe for Gal-ATM1/Glu/O_2 mitochondria in that the total carbonylated protein level was ~300% of the WT amount. The extent of damage was higher than reported for mitochondria isolated from the *yfh1*Δ strain (~250% relative to WT) (*31*). The extent of oxidative damage appeared proportional to the amount of hyperaccumulated Fe, with mitochondria from galactose-grown cells exhibiting less ROS damage and less Fe accumulation than those from glucose-grown cells. As expected, the level of ROS damage was less in W303 and Gal-ATM1 cells grown under anaerobic conditions (Figure 9, lanes 5 and 6).

DISCUSSION

No ISC Phenotype in Atm1p-Depleted Mitochondria from Anaerobic Cells. In this study, we have used an integrative biophysical approach to characterize the Fe in Atm1p-depleted mitochondria. Our results indicate that under anaerobic growth conditions Atm1p-depleted mitochondria contain WT levels of Fe/S clusters and heme groups and do not hyperaccumulate Fe. Since heme synthesis is O_2-dependent, the WT level of hemes in anaerobic cells is substantially reduced relative to that in aerobically grown cells. In terms of mitochondrial ISC and heme centers, such mitochondria cannot be distinguished from mitochondria of WT cells grown anaerobically. This indicates that *Atm1p is not required for mitochondrial Fe/S cluster assembly or heme biosynthesis*.

In anaerobic cells, lack of Atm1p in the mitochondria does not appear to perturb the mechanism that regulates the import flux of Fe into the mitochondria. In aerobic cells, this mechanism involves Aft1p, Aft2p, Fet3p, and other proteins of the iron regulon and other iron-responsive genes (*5*). The Atm1p-exported species X has been proposed to regulate this system, with a deficiency of cytosolic X (e.g., caused by a deficiency of Atm1p) upregulating the import of Fe into the cell and subsequently into mitochondria (see the model of Hausmann *et al.* (*5*)). Taken at face value, our results appear inconsistent with this proposal; however, the mechanism that regulates Fe in anaerobic cells is different. In anaerobic yeast cells, Hassett *et al.* (*32*) have shown that the high-affinity Fe transporter system (Fet3p) is significantly repressed and not functioning; instead, the low-affinity transporter (Fet4p) is upregulated and serves as the major cellular Fe uptake pathway (*33*). Fet4p is transcriptionally regulated by Aft1p and Rox1p and the cytosolic Fe status (via an unknown mechanism); however, it appears to have an effective posttranslational regulation so that its Fe uptake is actually independent of Aft1p (*34*); rather, the cytosolic Fe status seems to be the only decisive factor for Fe uptake rate for anaerobic cells. Thus, our results indicate that Atm1p and X are not involved in regulating iron uptake in *anaerobic* cells; i.e., X is not a sensor for Fe regulation under anaerobic conditions. Our results have no bearing on whether X is the sensor for the *AFT1*/*AFT2*-based iron regulon system.

Iron−Sulfur Cluster and Heme Defects in Atm1p-Depleted Mitochondria Isolated from Aerobic Cells. The spectra presented here reveal that the concentrations of ISCs and heme groups in Atm1p-depleted mitochondria from aerobically grown cells are significantly (4−8-fold) reduced relative to WT mitochondria grown under the same conditions. For ISCs, this was confirmed by aconitase and succinate dehydrogenase activities which were significantly reduced in Atm1p-depleted mitochondria, relative to that of WT cells. We cannot exclude the presence of *some* ISC- and heme-containing proteins in Atm1p-depleted mitochondria, but there is no doubt that there is an ISC defect in the organelle and that the levels of these clusters are diminished relative to those in WT mitochondria.

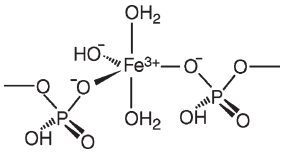

FIGURE 10: Candidate structure for the ferric nanoparticles in Atm1p-depleted mitochondria. Other 5-coordinate geometries besides the suggested trigonal bipyramidal are possible. Other protonation states for water and hydroxide ligands are also possible, as long as overall charge neutrality is maintained.

This contrasts with previous studies (*6*, *7*) which concluded that there is no defect in ISC assembly in Atm1p-depleted mitochondria (from aerobic yeast cells). These studies were based solely on the activity of various Fe/S cluster-containing enzymes; they did not involve a biophysical investigation. Actually, these studies also found reduced ISC levels in yeast mitochondria depleted in Atm1p or homologues, but the degree of reduction was regarded as being insufficient to conclude that there was an ISC assembly defect. Using HeLa cells in which the homologue *ABCB7* had been knocked down to 20−30% of WT level, Cavadini *et al.* (*35*) found that mitochondrial and cytosolic aconitase activities were ~50% and ~20% of control values, respectively, and that the activity of succinate dehydrogenase, a mitochondrial enzyme, was ~80% of WT level. They implied that there is no significant ISC defect in the mitochondria and suggested that ABCB7 exports Fe from the mitochondria to the cytosol.

Differences in mitochondrial Fe/S-containing enzyme activities and ISC levels in yeast cells may arise from differences in the growth media and the extent of Atm1p depletion. Atm1p-deleted cells do not grow on minimal media but grow slowly on rich media (*3*). Atm1p-depleted cells grow on minimal media, but they contain reduced levels of hemes relative to rich media levels (*5*). Growth on minimal medium may stress cells and result in a more complete depletion of Atm1p and perhaps some additional secondary phenotypes. Differences in growth times may have also influenced outcomes, as shutting down *ATM1* expression is a slow process that occurs over the course of tens of hours (*7*).

Role of O_2 in the Development of the ISC Defect in Atm1p-Depleted Mitochondria. The presence of ISCs in mitochondria from anaerobic cells suggests that such clusters are *assembled* in mitochondria from aerobic cells but that they are rapidly degraded such that steady-state levels of these clusters are low. Our results show that high levels of reactive oxygen species (ROS) are generated in Atm1p-depleted mitochondria from aerobic cells. We have also discovered that high-spin Fe(II) ions accumulate in Atm1p-depleted mitochondria (see below). Although nothing is known about the properties of these ions, mononuclear high-spin Fe(II) ions are known to engage in Fenton chemistry to generate ROS (*36*). ISCs in Atm1p-depleted mitochondria may be degraded by reaction with O_2 or ROS generated in this way, similar to that found in other systems (*37*). Inorganic synthesis of ISCs or reconstitution of such centers on proteins generally requires anaerobic conditions. Oxygen exposure in isolated yeast mitochondria inhibits one or several steps in ISC assembly (*38*). The reduction in heme centers could be similarly rationalized, as originally suggested by Kispal *et al.* (*6*).

Characterization of Ferric Nanoparticles in Atm1p-Depleted Mitochondria. In this study, we found that the Fe which hyperaccumulates in Atm1p-depleted mitochondria is in the form of ferric phosphate nanoparticles. We have characterized these nanoparticles in some detail. EPR and Mössbauer spectra

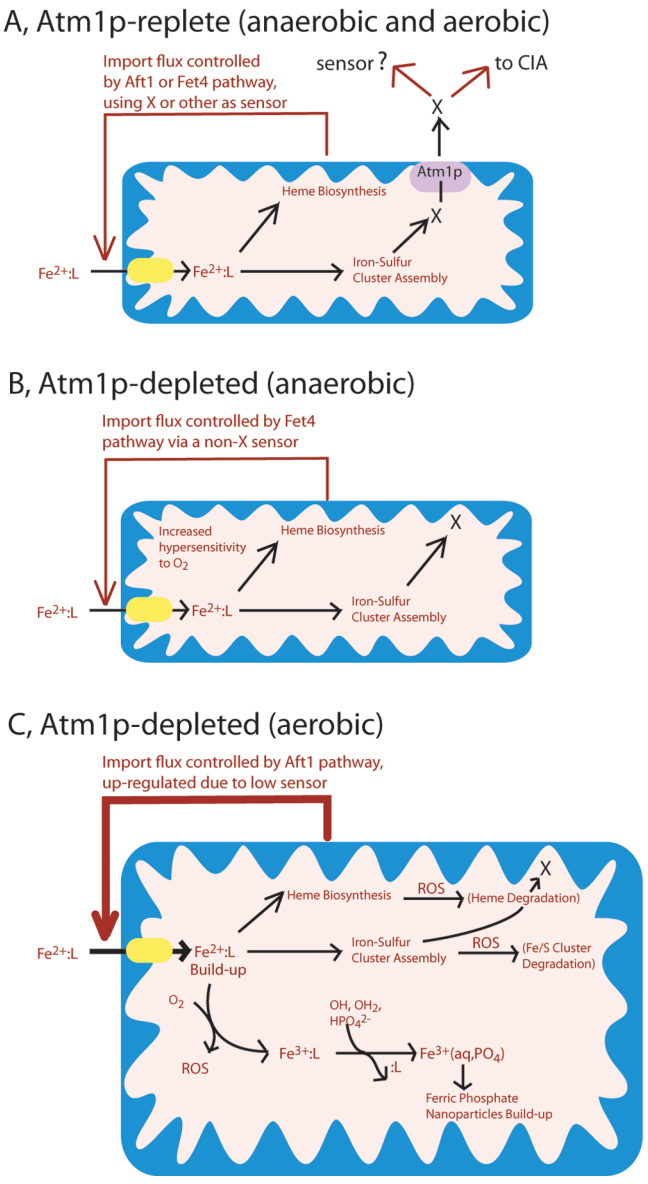

FIGURE 11: Working model for the effects of Atm1p depletion. The red line indicates a regulatory feedback mechanism in which the Fe status within the mitochondria is somehow sensed by the *AFT1*/*AFT2* system in aerobic cells and by the *FET4* system in anaerobic cells. See text for other details.

indicate superparamagnetically relaxing, magnetically interacting ferric ions, similar to that observed in Yah1p-depleted (*11*) and Yfh1p-deleted (*10*) mitochondria. EM images reveal individual particles 2−4 nm in diameter, clumped into larger aggregates. Our EM results show nanoparticles composed of Fe and P in approximately equimolar amounts.

Phosphate ions are present at high concentration in the mitochondrial matrix (estimated between 10 and 20 mM) (*39*), and this is almost certainly the form of phosphorus detected in the nanoparticles. For Fe−O−P(phosphate) units, Fe−O and O−P bond distances of 2.01 and 1.53 Å are commonly observed (*40*). By assuming a triangle with sides of length 2.01, 1.53, and 3.21 Å (the latter corresponding to the Fe−P length determined by EXAFS), the law of cosines indicates 130° for the Fe−O−P angle. This excludes a linear arrangement for these atoms. Bidentate coordination of Fe to two oxygen atoms from the same phosphate ion is also excluded, as this would require a shorter Fe−P distance (≤2.46 Å) than is observed.

The other ligands coordinating the ferric ions in the nanoparticles are unknown, but our EM results indicate that they involve oxygen atoms but probably not nitrogen, sulfur, or carbon atoms. These results, along with the observed average Fe−O bond distance of 1.97 Å, suggest a combination of water/hydroxide ligands. The Fe−O bond distances in Fe(III)−OH and Fe(III)−OH_2 arrangements are 1.91 and 2.05 Å, respectively (*41*). A charge-neutral 5-coordinate ferric site with two Fe−O bonds (from phosphate) at 2.01 Å, one Fe−OH bond at 1.91 Å, and two Fe−OH_2 bonds at 2.05 Å would have an average Fe−O bond length of 2.01 Å, slightly longer than the observed value of 1.97 Å, but near to the uncertainty of the EXAFS measurement. The Debye−Waller factor estimated from this disordered set of ligands of 0.003 $Å^2$ is somewhat smaller that the observed value of 0.0055 $Å^2$. Nevertheless, the difference is perhaps within the uncertainty of the measurement. A candidate ferric nanoparticle structure satisfying all of these relationships is shown in Figure 10.

The ferric ions in these nanoparticles were likely imported by passage through an IM transporter such as Mrs3p or Mrs4p (or by another unidentified low- or high-affinity Fe transporter) in the form of Fe(II) ions (*42*). Regardless of the transporter, the mechanism of import likely involves the transporter recognizing the structure of the low molecular Fe(II) trafficking complex. Consider that the imported Fe(II) ions are coordinated by an unknown endogenous ligand L whose structure is recognized by the IM transporter. It seems unlikely that Fe(II):L would be "free" (i.e., hexaqua) ferrous ions as this would not provide the necessary discrimination required for trafficking. Moreover, hexaqua ferrous complexes are highly susceptible to oxidation and precipitation, and they could engage in Fenton chemistry that would damage the cell. Thus, we propose that L consists of species other than waters or hydroxide ions. This suggests that once these Fe(II):L complexes are imported into the matrix, *the process of nanoparticle formation is initiated by oxidation to Fe(III) and the exchange of L for waters/hydroxide/phosphate ions*. The resulting Fe(III) species would precipitate into nanoparticles. This model is illustrated in Figure 11C.

High-Spin Ferrous Ions in Mitochondria from Atm1p-Depleted and Yah1p-Depleted Cells. We have discovered that mitochondria from aerobically grown cells that are depleted in either Atm1p or Yah1p also accumulate nonheme high-spin Fe(II) ions. The concentration of such ions within these organelles is substantial; we estimate 300−500 μM for Atm1p fully depleted, 50 μM for Atm1p partially depleted, and ~150 μM for Yah1p-depleted mitochondria. Such ions are also present in whole Atm1p-depleted cells. Nonheme HS Fe(II) ions are present in mitochondria from WT cells (data not shown) but at lower levels. Interestingly, no such ions appear to be present in Yfh1p-depleted mitochondria (*10*), suggesting that this may be a distinguishing property of the ISC phenotype. Further studies are required to explore this possibility.

We have characterized these accumulated Fe(II) complexes preliminarily. The line width of the HS Fe(II)-associated doublet from mitochondria of Gal-ATM1/Glu/O_2 cells was about twice that of the same doublet associated with Gal-ATM1/Gal/O_2 cells. The line width of the HS Fe(II) doublet of mitochondria of glucose-grown cells was so large as to suggest that more than one species contributes. Mitochondria from Atm1p partially depleted cells grown on galactose could contain a single HS Fe(II) complex. None of these species appears to be hexaqua Fe(II) ions.

Function of Atm1 and X. Given the complexity of cells, determining the exact cellular functions of Atm1p and X is exceedingly difficult, with limited number of experimental results to guide us. Two functions for Atm1p and X have been suggested (*5*). One links mitochondrial ISC assembly to cytosolic ISC assembly (CIA). X would be produced in proportion to the rate of mitochondrial ISC assembly and exported into the cytosol where it would serve either as a substrate or as a cocatalyst for CIA-dependent ISC assembly. When mitochondria would be depleted in Atm1p, X would not be exported, halting cytosolic ISC assembly but not mitochondrial ISC assembly. Our results show a defect in mitochondrial Fe/S clusters under aerobic conditions but not under anaerobic conditions. We interpret this to mean that ISC's *are* assembled in Atm1p-depleted mitochondria but that they are rapidly degraded by ROS under aerobic conditions. These results are consistent with the previously proposed function of Atm1p/X, which imply that Atm1p is not involved in mitochondrial Fe/S cluster assembly.

We also considered whether the ROS generated in this process, rather than the lack of X in the cytosol, might be responsible for the lack of CIA-dependent Fe/S cluster assembly in Atmp1-depleted cells. However, the absence of Leu1p activity in Atm1p-depleted cells grown under anaerobic conditions eliminates this possibility. Rather, this result provides independent evidence supporting the hypothesis that CIA-dependent ISC assembly requires X as a substrate or catalyst.

Kispal *et al.* (*7*) cautiously suggested that X might contain both sulfur and iron and that the accumulated Fe in Atm1p-deleted mitochondria might be X itself (*7*, *43*). Other researchers have suggested this possibility as well (*44*−*46*). Our results demonstrate that the accumulated Fe is ferric phosphate nanoparticles, inconsistent with this suggestion.

The second proposed function of X is to communicate the status of mitochondrial ISC assembly to the Aft1p-controlled iron regulon and other iron-responsive genes (*5*). Here, the presence of cytosolic X would signal to the Aft1p-controlled system that mitochondrial ISC assembly is functioning properly. Accordingly, a deficiency of cytosolic X would alert the system of depressed rates of mitochondrial ISC assembly, prompting an increased import flux of Fe into cells and probably into mitochondria. Our results show that this flux is not increased in Atm1p-depleted anaerobic cells, but this has no bearing on this proposed function for Atm1p/X, in that the *AFT1*/*AFT2*-based iron regulon is not the primary regulator of cellular Fe under anaerobic conditions.

Model for the Development of the ISC Phenotype in Atm1p-Depleted Cells. Our study has shown that the phenotypes for mitochondria obtained from Atm1p-depleted and Yah1p-depleted cells are largely indistinguishable, at least when grown under aerobic conditions on minimal medium. The recent study of Hausmann *et al.* (*5*) supports this conclusion. In that study, a microarray analysis of the transcriptome of Yah1p-depeleted and Atm1p-depleted yeast cells revealed significant differences in expression levels of ~200 genes relative to WT cells, but the changes in expression levels of these genes were rather similar (not identical) for both strains. This makes it difficult to correlate the ISC phenotype to the functions of proteins the lack of which cause the phenotype. Also, since there are many aspects to that phenotype, primary and secondary effects cannot be easily distinguished. Thus, proteins affording the ISC phenotype may primarily alter other aspects of

metabolism (e.g., involving sulfur, oxygen, cellular redox homeostasis and/or regulation), and the observed effects on Fe metabolism may be secondary effects.

Despite these difficulties, it is interesting to consider the sequence of events that might lead to the ISC phenotype. We found here that the contents and distribution of Fe in WT and Atm1p-depleted cells are essentially indistinguishable under anaerobic conditions (Figure 11B) but dramatically different under aerobic conditions. WT aerobic cells show little response to O_2 exposure (Figure 11A) while the mutant strains show several strong phenotypes including the ISC defect. Thus, we suggest that Atm1p depletion (and Yah1p depletion) increases the cell's *sensitivity* to O_2 exposure. According to the model of Figure 11C, Fe(II):L in Atm1p-depleted mitochondria is easily oxidized to Fe(III):L in the presence of O_2 (somehow this does not happen in WT cells). This generates ROS (directly or indirectly) and prompts L, assumed to prefer Fe(II) coordination, to dissociate. Under these conditions, ISCs and perhaps heme groups are synthesized but are degraded quickly as they react with the newly generated ROS.

Hyperaccumulation of Iron. "Free" Fe(III) ions are essentially insoluble at neutral and alkaline pHs and, according to our model, would rapidly precipitate in the mitochondrial matrix to form nanoparticles. These nanoparticles accumulate beyond the level of Fe that is typically found in WT mitochondria, suggesting that the formation of nanoparticles is likely associated with an increased flux of Fe(II):L ions into the matrix, probably as a homeostatic regulatory response. We previously suggested that Fe regulation operated at the level of mitochondria (e.g., where the concentration of HS Fe(II) ions in the mitochondrial matrix served as a sensor to regulate import flux) (*11*). However, the high levels of HS Fe(II) ions present in the mitochondria that are experiencing this increased import flux could be used to argue against this. One possibility is that the particular HS Fe(II) complex (or complexes) formed under these circumstances is (are) not the particular HS Fe(II) complex(es) that is (are) sensed. Another possibility, which we regard as more likely, is that mitochondrial Fe(II):L import flux is regulated at the cellular level via *AFT1*/*AFT2* and the iron regulon and that the sensor is something other than Fe(II):L. In this model, regulation would still involve a species whose concentration reflects the Fe status within the mitochondria (e.g., X; see above). Changes in the concentration of this sensor would be monitored (directly or indirectly) by the *AFT1*/*AFT2* system, ultimately affecting the import flux of Fe(II):L. The sensor's concentration might change as a response to either Fe(II) oxidation, ligand exchange, or nanoparticle formation. Besides X, a molecule oxidized by ROS or the ligand L that is released during exchange should be viewed as candidates for this sensor. The nanoparticles themselves are probably chemically inert and thus unlikely to be the sensor. Moreover, the sensor would need to be exported from the mitochondria and to interact with the *AFT1*/*AFT2* system, roles that nanoparticles could not play.

Further evidence for a cellular (rather than organellar) level response to the Atm1p-dependent changes occurring within the organelle is provided by the massive alteration of the Fe content of whole WT cells vs whole Gal-ATM1/Glu/O_2 cells. Although much work remains to understand these changes, it is clear that a deficiency of Atm1p in the IM of the mitochondria has global consequences, ultimately influencing Fe metabolism throughout the cell.

ACKNOWLEDGMENT

We thank Marlène Martinho and Eckard Münck (Carnegie Mellon University) for collecting the high-field Mössbauer spectrum presented in the text and Joseph Reibenspies for helpful discussion regarding Fe−ligand bond distances.

SUPPORTING INFORMATION AVAILABLE

XAS data and fits to various models. This material is available free of charge via the Internet at http://pubs.acs.org.

REFERENCES

1. Labbebois, R. (1990) The ferrochelatase from *Saccharomyces cerevisiae*—Sequence, disruption, and expression of its structural gene Hem15. *J. Biol. Chem. 265*, 7278–7283.
2. Lill, R., and Mühlenhoff, U. (2008) Maturation of iron-sulfur proteins in eukaryotes: Mechanisms, connected processes, and diseases. *Annu. Rev. Biochem. 77*, 669–700.
3. Leighton, J., and Schatz, G. (1995) An ABC transporter in the mitochondrial inner membrane is required for normal growth of yeast. *EMBO J. 14*, 188–195.
4. Kuhnke, G., Neumann, K., Mühlenhoff, U., and Lill, R. (2006) Stimulation of the ATPase activity of the yeast mitochondrial ABC transporter Atm1p by thiol compounds. *Mol. Membr. Biol. 23*, 173–184.
5. Hausmann, A., Samans, B., Lill, R., and Mühlenhoff, U. (2008) Cellular and mitochondrial remodeling upon defects in iron-sulfur protein biogenesis. *J. Biol. Chem. 283*, 8318–8330.
6. Kispal, G., Csere, P., Guiard, B., and Lill, R. (1997) The ABC transporter Atm1p is required for mitochondrial iron homeostasis. *FEBS Lett. 418*, 346–350.
7. Kispal, G., Csere, P., Prohl, C., and Lill, R. (1999) The mitochondrial proteins Atm1p and Nfs1p are essential for biogenesis of cytosolic Fe/S proteins. *EMBO J. 18*, 3981–3989.
8. Guarente, L., and Mason, T. (1983) Heme regulates transcription of the Cyc1 gene of *S. cerevisiae* via an upstream activation site. *Cell 32*, 1279–1286.
9. Lange, H., Mühlenhoff, U., Denzel, M., Kispal, G., and Lill, R. (2004) The heme synthesis defect of mutants impaired in mitochondrial iron-sulfur protein biogenesis is caused by reversible inhibition of ferrochelatase. *J. Biol. Chem. 279*, 29101–29108.
10. Lesuisse, E., Santos, R., Matzanke, B. F., Knight, S. A. B., Camadro, J. M., and Dancis, A. (2003) Iron use for haeme synthesis is under control of the yeast frataxin homologue (Yfh1). *Hum. Mol. Genet. 12*, 879–889.
11. Miao, R., Martinho, M., Morales, J. G., Kim, H., Ellis, E. A., Lill, R., Hendrich, M. P., Münck, E., and Lindahl, P. A. (2008) EPR and Mössbauer spectroscopy of intact mitochondria isolated from Yah1p-depleted *Saccharomyces cerevisiae*. *Biochemistry 47*, 9888–9899.
12. Kaplan, J., Ward, D. M., Crisp, R. J., and Philpott, C. C. (2006) Iron-dependent metabolic remodeling in *S. cerevisiae*. *Biochim. Biophys. Acta 1763*, 646–651.
13. Rutherford, J. C., Ojeda, L., Balk, J., Mühlenhoff, U., Lill, R., and Winge, D. R. (2005) Activation of the iron regulon by the yeast Aft1/Aft2 transcription factors depends on mitochondrial but not cytosolic iron-sulfur protein biogenesis. *J. Biol. Chem. 280*, 10135–10140.
14. Hanikenne, M., Motte, P., Wu, M. C. S., Wang, T., Loppes, R., and Matagne, R. F. (2005) A mitochondrial half-size ABC transporter is involved in cadmium tolerance in *Chlamydomonas reinhardtii*. *Plant Cell Environ. 28*, 863–873.
15. Csere, P., Lill, R., and Kispal, G. (1998) Identification of a human mitochondrial ABC transporter, the functional orthologue of yeast Atm1p. *FEBS Lett. 441*, 266–270.
16. Bekri, S., Kispal, G., Lange, H., Fitzsimons, E., Tolmie, J., Lill, R., and Bishop, D. F. (2000) Human ABC7 transporter: gene structure and mutation causing X-linked sideroblastic anemia with ataxia with disruption of cytosolic iron-sulfur protein maturation. *Blood 96*, 3256–3264.
17. Camaschella, C. (2008) Recent advances in the understanding of inherited sideroblastic anaemia. *Br. J. Hamaetol. 143*, 27–38.
18. Pondarre, C., Campagna, D. R., Antiochos, B., Sikorski, L., Mulhern, H., and Fleming, M. D. (2007) Abcb7, the gene responsible for X-linked sideroblastic anemia with ataxia, is essential for hematopoiesis. *Blood 109*, 3567–3569.

19. Hudder, B. N., Morales, J. G., Stubna, A., Münck, E., Hendrich, M. P., and Lindahl, P. A. (2007) Electron paramagnetic resonance and Mössbauer spectroscopy of intact mitochondria from respiring *Saccharomyces cerevisiae*. *J. Biol. Inorg. Chem. 12*, 1029–1053.
20. Lindahl, P., Morales, J. G., Miao, R., and Holmes-Hampton, G. (2009) Isolation of *Saccharomyces cerevisiae* mitochondria for Mössbauer, EPR, and electronic absorption spectroscopic analyses. *Methods Enzymol. 456*, 267–285.
21. Schilke, B., Voisine, C., Beinert, H., and Craig, E. (1999) Evidence for a conserved system for iron metabolism in the mitochondria of *Saccharomyces cerevisiae*. *Proc. Natl. Acad. Sci. U.S.A. 96*, 10206–10211.
22. Kohlhaw, G. B. (1988) Isopropylmalate dehydratase from yeast. *Methods Enzymol. 166*, 423–429.
23. Munujos, P., Collcanti, J., Gonzalezsastre, F., and Gella, F. J. (1993) Assay of succinate-dehydrogenase activity by a colorimetric-continuous method using iodonitrotetrazolium chloride as electron-acceptor. *Anal. Biochem. 212*, 506–509.
24. Tamarit, J., Irazusta, V., Moreno-Cermeno, A., and Ros, J. (2006) Colorimetric assay for the quantitation of iron in yeast. *Anal. Biochem. 351*, 149–151.
25. Poiarkova, A. V., and Rehr, J. J. (1999) Multiple-scattering x-ray-absorption fine-structure Debye-Waller factor calculations. *Phys. Rev. B 59*, 948–957.
26. Plattner, H., and Schatz, G. (1969) Promitochondria of anaerobically grown yeast. 3. Morphology. *Biochemistry 8*, 339–343.
27. Kwast, K. E., Lai, L. C., Menda, N., James, D. T., Aref, S., and Burke, P. V. (2002) Genomic analyses of anaerobically induced genes in *Saccharomyces cerevisiae*: Functional roles of Rox1 and other factors in mediating the anoxic response. *J. Bacteriol. 184*, 250–265.
28. Paltauf, F., and Schatz, G. (1969) Promitochondria of anaerobically grown yeast. 2. Lipid composition. *Biochemistry 8*, 335–339.
29. Rosenfeld, E., and Beauvoit, B. (2003) Role of the non-respiratory pathways in the utilization of molecular oxygen by *Saccharomyces cerevisiae*. *Yeast 20*, 1115–1144.
30. Barros, M. H., Nobrega, F. G., and Tzagoloff, A. (2002) Mitochondrial ferredoxin is required for heme A synthesis in *Saccharomyces cerevisiae*. *J. Biol. Chem. 277*, 9997–10002.
31. Bulteau, A. L., Dancis, A., Gareil, M., Montagne, J. J., Camadro, J. M., and Lesuisse, E. (2007) Oxidative stress and protease dysfunction in the yeast model of Friedreich ataxia. *Free Radical Biol. Med. 42*, 1561–1570.
32. Hassett, R. F., Romeo, A. M., and Kosman, D. J. (1998) Regulation of high affinity iron uptake in the yeast *Saccharomyces cerevisiae*—Role of dioxygen and Fe(II). *J. Biol. Chem. 273*, 7628–7636.
33. Jensen, L. T., and Culotta, V. C. (2002) Regulation of *Saccharomyces cerevisiae* FET4 by oxygen and iron. *J. Mol. Biol. 318*, 251–260.
34. Waters, B. M., and Eide, D. J. (2002) Combinatorial control of yeast FET4 gene expression by iron, zinc, and oxygen. *J. Biol. Chem. 277*, 33749–33757.
35. Cavadini, P., Biasiotto, G., Poli, M., Levi, S., Verardi, R., Zanella, I., Derosas, M., Ingrassia, R., Corrado, M., and Arosio, P. (2007) RNA silencing of the mitochondrial ABCB7 transporter in HeLa cells causes an iron-deficient phenotype with mitochondrial iron overload. *Blood 109*, 3552–3559.
36. Halliwell, B. (2009) The wanderings of a free radical. *Free Radical Biol. Med. 46*, 531–542.
37. Imlay, J. A. (2006) Iron-sulphur clusters and the problem with oxygen. *Mol. Microbiol. 59*, 1073–1082.
38. Mühlenhoff, U., Richhardt, N., Gerber, J., and Lill, R. (2002) Characterization of iron-sulfur protein assembly in isolated mitochondria—A requirement for ATP, NADH, and reduced iron. *J. Biol. Chem. 277*, 29810–29816.
39. Rauen, U., Springer, A., Weisheit, D., Petrat, F., Korth, H. G., de Groot, H., and Sustmann, R. (2007) Assessment of chelatable mitochondrial iron by using mitochondrion-selective fluorescent iron indicators with different iron-binding affinities. *ChemBioChem 8*, 341–352.
40. Cambridge Structural Database (http://www.ccdc.cam.ac.uk/products/csd/).
41. Wilkinson, E. C., Dong, Y. H., and Que, L. (1994) Modeling hydrolysis at dinuclear iron centers. *J. Am. Chem. Soc. 116*, 8394–8395.
42. Lange, H., Kispal, G., and Lill, R. (1999) Mechanism of iron transport to the site of heme synthesis inside yeast mitochondria. *J. Biol. Chem. 274*, 18989–18996.
43. Lill, R., and Mühlenhoff, U. (2006) Iron-sulfur protein biogenesis in eukaryotes: Components and mechanisms. *Annu. Rev. Cell. Dev. Biol. 22*, 457–486.
44. Schueck, N. D., Woontner, M., and Koeller, D. M. (2001) The role of the mitochondrion in cellular iron homeostasis. *Mitochondrion 1*, 51–60.
45. Burke, M. A., and Ardehali, H. (2007) Mitochondrial ATP-binding cassette proteins. *Transl. Res. 150*, 73–80.
46. Chen, S., Sanchez-Fernandez, R., Lyver, E. R., Dancis, A., and Rea, P. A. (2007) Functional characterization of AtATM1, AtATM2, and AtATM3, a subfamily of *Arabidopsis* half-molecule ATP-binding cassette transporters implicated in iron homeostasis. *J. Biol. Chem. 282*, 21561–21571.
47. Liu, W. T., and Thorp, H. H. (1993) Bond valence sum analysis of metal-ligand bond lengths in metalloenzymes and model complexes. 2. Refined distances and other enzymes. *Inorg. Chem. 32*, 4102–4105.